



# Microseismic Monitoring and Rockburst Characteristics in a Deep-Buried Tunnel Excavated by TBM

Qi Zhang<sup>1</sup> · Xiao-Ping Zhang<sup>1</sup> · Quansheng Liu<sup>1</sup> · Yucong Pan<sup>1</sup> · Jianjun Chi<sup>2</sup> · Junbo Qiu<sup>1</sup> · Xin Yin<sup>1</sup>

Received: 1 June 2023 / Accepted: 26 October 2023 / Published online: 17 December 2023  
© The Author(s), under exclusive licence to Springer-Verlag GmbH Austria, part of Springer Nature 2023

## Abstract

Rockbursts have become one of the main engineering disasters in deep-buried tunnel, seriously threatening the safety of worker and equipment. To monitor microseismic (MS) events and predict rockburst, in the present study, a MS monitoring system was established in a deep-buried tunnel excavated by tunnel boring machine (TBM). Characteristics of MS events were studied and a prediction method for intense rockburst was proposed by analyzing the temporal–spatial distribution, source parameters, and failure mechanism. The results indicated that most of MS events occurred during the tunneling process and within 15 min after a tunneling cycle completed. The MS events mainly distributed within 15 m before and after the tunneling face, and within approximate 2.0 times of the tunnel diameter. The energy of these MS events mainly ranged from 30 to 100 kJ. The prediction method based on cumulative energy index of per day and cumulative apparent volume cannot predict intense rockburst accurately in the present study, the forecast accuracy less than 60%. The proposed prediction index based on the energy index of per MS event and the apparent volume of per MS event can effectively sharpen the forecast accuracy (> 85%). The failure mechanism of MS events was predominated by tensile failure. While as the rockburst segment transited from mild to intense, the percentage of MS events of mixed failure and shear failure increased, especially shear failure events.

## Highlights

- The temporal and the spatial distribution characteristics of rockburst segment in a deep-buried tunnel were revealed.
- Microseismic event count, energy, energy index, apparent volume, failure mechanism, and the development process of mild, moderate, and intense rockburst segments were studied.
- A prediction index based on energy index and apparent volume of per microseismic event was proposed to forecast intense rockburst.

**Keywords** Tunnel boring machine · Deep-buried tunnel · Rockburst · Microseismic monitoring · Warning

## 1 Introduction

Numerous deep-buried underground projects are under construction or planned in China, involving water diversion, mining, traffic, hydropower and national defense engineering. As the buried depth increases, in situ stress increases and geological conditions become more complicated (Chen et al. 2020, 2021; Dai et al. 2017). Under the influence of excavation disturbance, hard and brittle surrounding rocks tend to break and induce engineering disasters, e.g., spalling, collapse, and rockburst (Cai et al. 2001; Roy et al. 2023; Si et al. 2023). Rockburst, a dynamic disaster, defines the sudden or violent collapse of rock mass with the sound and

✉ Xiao-Ping Zhang  
jxhkzhang@163.com

Qi Zhang  
zhqi@whu.edu.cn

<sup>1</sup> Key Laboratory of Safety for Geotechnical and Structural Engineering of Hubei Province, School of Civil Engineering, Wuhan University, Wuhan 430072, China

<sup>2</sup> China Water Resources Beifang Investigation, Design & Research Co. Ltd, Tianjin 300222, China

ejected rock fragments (Kaiser et al. 1996; Najm and Daraei 2023; Feng et al. 2013; Su et al. 2023; Xiao et al. 2016a). It usually leads to equipment damages, project delays, economic losses, even serious casualties (Małkowski and Niedbalski 2020; Lu et al. 2018; Xu et al. 2017; Zhou et al. 2018). At present, rockburst has become one of the major disasters in deep-buried underground project, especially for the project with deep-buried depth.

A large number of researches have been conducted to study evolution characteristics and mitigation strategies. Ortlepp (2000) discussed the extremely violent fracturing phenomena, and indicated that the rockburst rupture was a microcosm of the pristine earthquake. The microseismic (MS) monitoring technique was adopted to monitor and warn the rockburst, such as Jinping II hydropower station (Feng et al. 2015), Gotthard Base tunnel (Rehbock-Sander and Jesel 2018), and Hanjiang–Weihe River diversion tunnel (Zhu et al. 2019), etc. Analyzing the active microseismicity, such as occurrence time, location, and intensity, potential rockburst areas can be identified (Feng et al. 2019; Xiao et al. 2016b; Xu et al. 2016; Yao et al. 2023). Moreover, through the interpretation of MS wave information, fracturing process of rock mass and failure mechanism can be investigated (Dai et al. 2016; Gibowicz et al. 1991; Tang et al. 2018; Wang et al. 2021). Then, development process and evolution mechanism of rockbursts can be revealed.

Previous researches mainly using the MS monitoring technique studied a case or several cases of rockbursts. Few researches studied the MS characteristics of a certain mileage segment. In the present study, a moveable MS monitoring system was installed in a tunnel boring machine (TBM) excavated diversion tunnel. The MS characteristics

of 500 m mileage segment (1266 MS events) were analyzed in detail. The temporal–spatial distribution of these MS events was analyzed. Then, the MS information, including MS energy, energy index, apparent volume, and failure mechanism, was quantitatively analyzed to investigate development process and evolution mechanism of rockbursts. The relationship between rockburst and induced microseismicity was revealed. The potential failure zone and the rockburst precursor were identified. A prediction index based on the energy index and apparent volume was proposed to predict intense rockburst. The results of present study can provide significant references for rockburst forewarning in deep-buried tunnels.

## 2 Engineering Background

### 2.1 Project Overview

The tunnel is located in northwestern China, and is approximately 41.8 km long. Approximately 32 km was excavated by TBM (Fig. 1). The mileages studied in the present study range from K31 + 930 to K31 + 430 (buried depth approximately 1170 m). The region is characterized by Variscan orogeny. The rock type mainly consists of granodiorite and granite. The squeeze folds and faults were developed. There were mainly two groups of steep faults in the present study areas, named SF17 and F32. Several rock samples were taken from the mileage of K31 + 368. The rock type of surrounding rock is granite. The physical–mechanical parameters of the granite is listed in Tables 1 and 2. A hydraulic fracturing method was adopted to measure the in situ stress

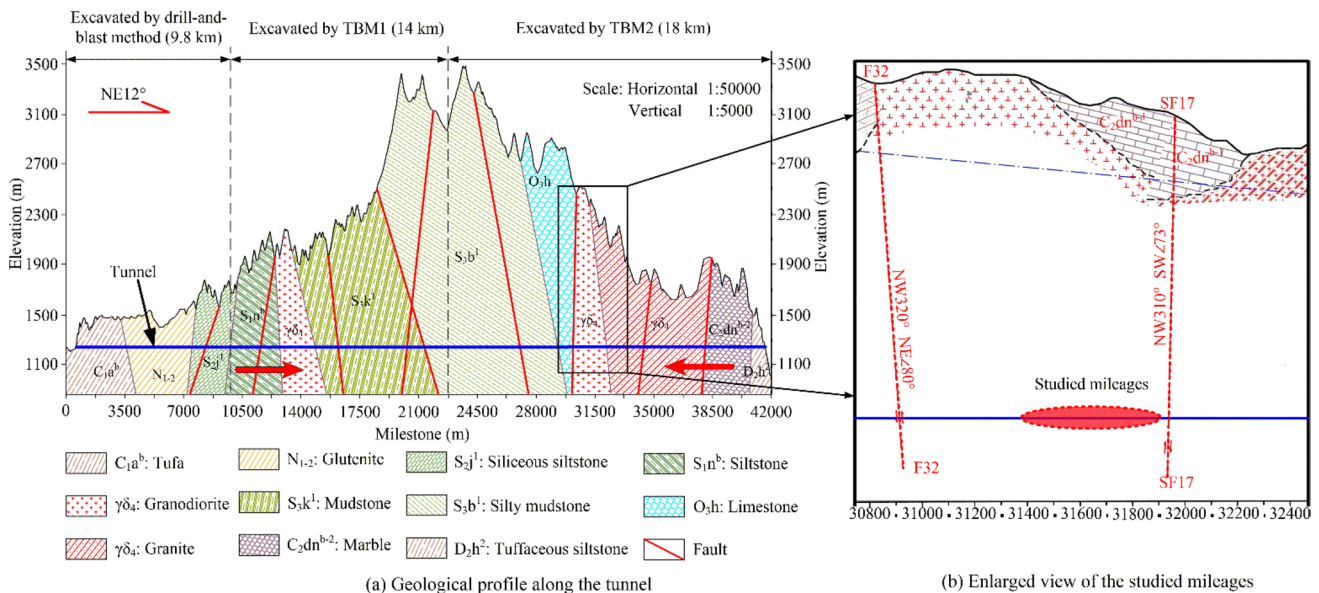


Fig. 1 Geological profile of the tunnel. Modified from Liu et al. (2020)

**Table 1** Physical–mechanical parameters of granite (uniaxial compressive test)

Specimen no.	Weight (g)	Height (mm)	Diameter (mm)	Density (g/cm <sup>3</sup> )	Wave velocity (km/s)	UCS (MPa)	Elasticity modulus (GPa)	Poisson’s ratio
1	510.20	100.09	49.96	2.60	4.18	161.07	60.87	0.37
2	512.30	100.04	49.97	2.61	4.56	187.22	68.11	0.37

**Table 2** Physical–mechanical parameters of granite (Brazilian test)

Specimen no.	Weight (g)	Height (mm)	Diameter (mm)	Density (g/cm <sup>3</sup> )	Wave velocity (km/s)	Tensile strength (MPa)
1	127.80	25.08	49.98	2.60	4.59	6.08
2	127.90	25.05	50.08	2.59	4.08	6.30
3	128.00	25.05	50.05	2.60	4.08	4.03

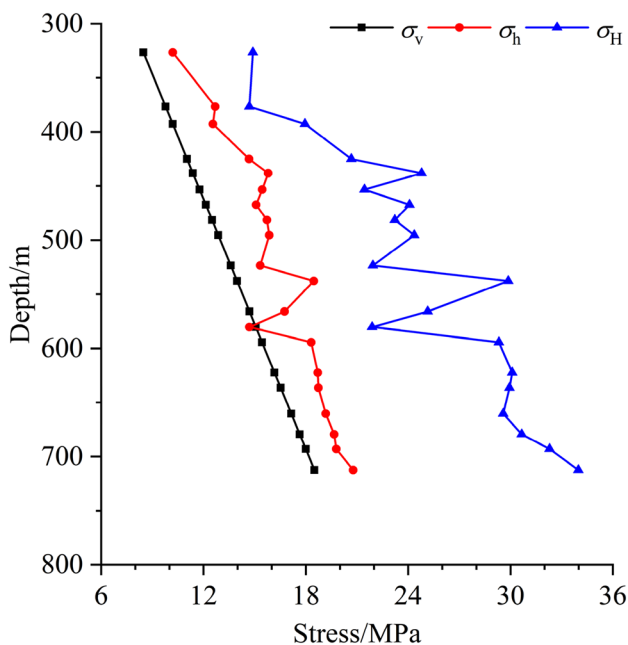


**Fig. 2** In situ stress measured by a hydraulic fracturing method in mileage K31+066, with a buried depth 720 m.  $\sigma_v$ ,  $\sigma_h$ , and  $\sigma_H$  represent respectively vertical principal stress, minimum horizontal principal stress, and maximum horizontal principal stress

at the mileage K31+066, with a buried depth 720 m. The result shows in Fig. 2. According to the data, the relationship between buried depth and in situ stress can be obtained. The buried depth of the studied mileage in the present study is approximately 1170 m. The  $\sigma_v$ ,  $\sigma_h$ , and  $\sigma_H$  of the studied mileage are respectively 30.38 MPa, 30.85 MPa, and 53.68 MPa.

Due to high in situ stress and high rock strength, rockbursts frequently occur, mainly moderate and intense levels. The rockburst level is determined according to the Code

for Geologic Investigation of Hydropower Engineering that is proposed by the National Standards Compilation Group of the People’s Republic of China (GB50487-2008) (China 2008). There were 1266 MS events recorded on the mileage of from K31+930 to K31+430 (Fig. 3a). Based on the location and the frequency of these MS events, the mileages are divided into three segments: mild rockburst segment (325 m), moderate rockburst segment (54.6 m), and intense rockburst segment (120.4 m) (Fig. 3b). Although some measurements had been carried out, such as water infusion, reducing tunneling rate, using 22-mm-diameter grouted rebar, 16-mm-diameter pre-fabricated reinforcing mesh, and H150 steel arch, several intense rockbursts occurred and caused some damages to the supporting system (Fig. 4). During these rockbursts, a considerable number of rock fragments were ejected from the surrounding rocks. The depth of these rockburst pits is larger than 1.0 m. Sometimes, reinforcing mesh was upheaval and breakage. The H150 steel arch was warped and dislocated. It took a large number of time to clean up these rock mass fragments and to replace these reinforcing meshes and steel arches. It seriously reduced the tunneling efficiency.

**2.2 MS Monitoring**

An MS monitoring system was established to acquire MS information in real time. The system consists of Paladin data acquisition system, Hyperion digital signal processing system, and six uniaxial accelerometers. The acquisition system has a sampling frequency of 10 kHz and a 24-bit analog-to-digital (A/D) converter. The frequency response of the uniaxial accelerometer ranges from 50 Hz to 5 kHz with a sensitivity of 30 V/g. The Paladin data acquisition system and the portable laptop were placed in a metal box (Fig. 5a). The accelerometers were placed 80 m behind the tunneling



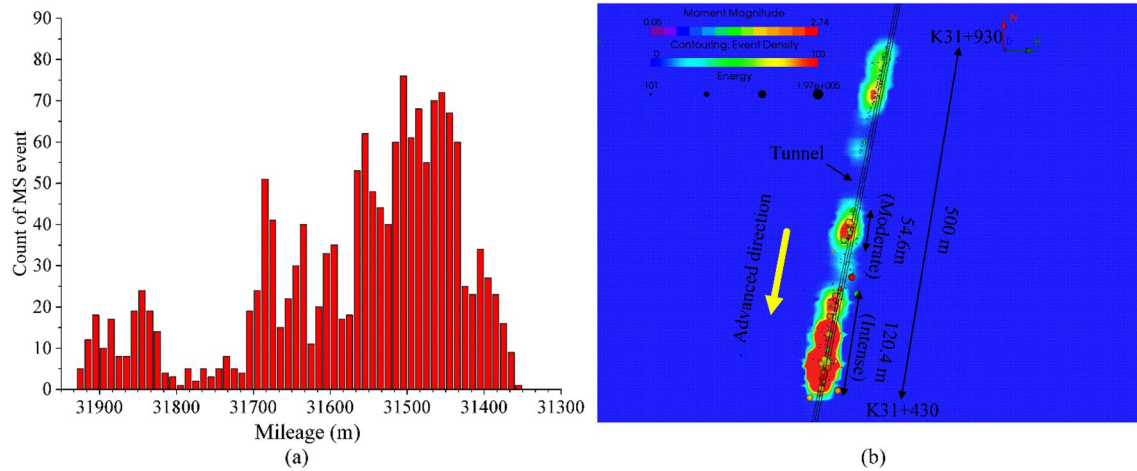


**Fig. 3** MS event information: **a** MS event distribution along the mileage; **b** MS even density contour

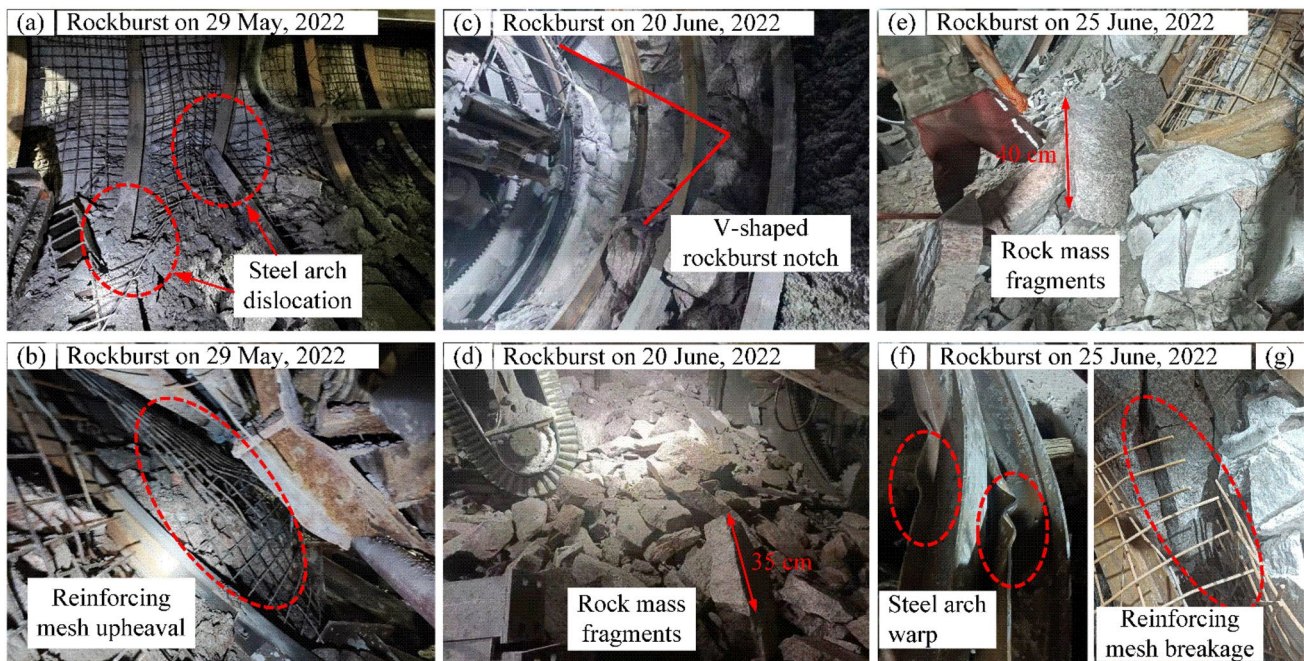


**Fig. 4** Photographs of rockbursts: **a, b** rockburst occurring on 29 May, 2022; **c, d** rockburst occurring on 20 June, 2022; **e, f** rockburst occurring on 25 June, 2022

face (Fig. 5b). There are three accelerometer arrays with an interval of 30 m. When the tunneling face moves 30 m forward, the two accelerometers of the last accelerometer array were retrieved and moved forward.

When MS events occurred, accelerometers receive these waveform signals that are converted into digital signals. Then, these digital signals are processed by the Hyperion digital signal processing system, including HNAS (hyperion network acquisition system), WaveVis

(waveform visualizer), and SeisProc™ (seismic processing software). The HNAS removes noise from waveform signal, and identifies the initial pulse of P waves and S waves. The WaveVis is a visualization software that can graphically display the seismic waveforms. Then, the source parameters of MS events are calculated through the SeisProc™, e.g., the location, energy, apparent volume, apparent stress, stress drop and moment magnitude.

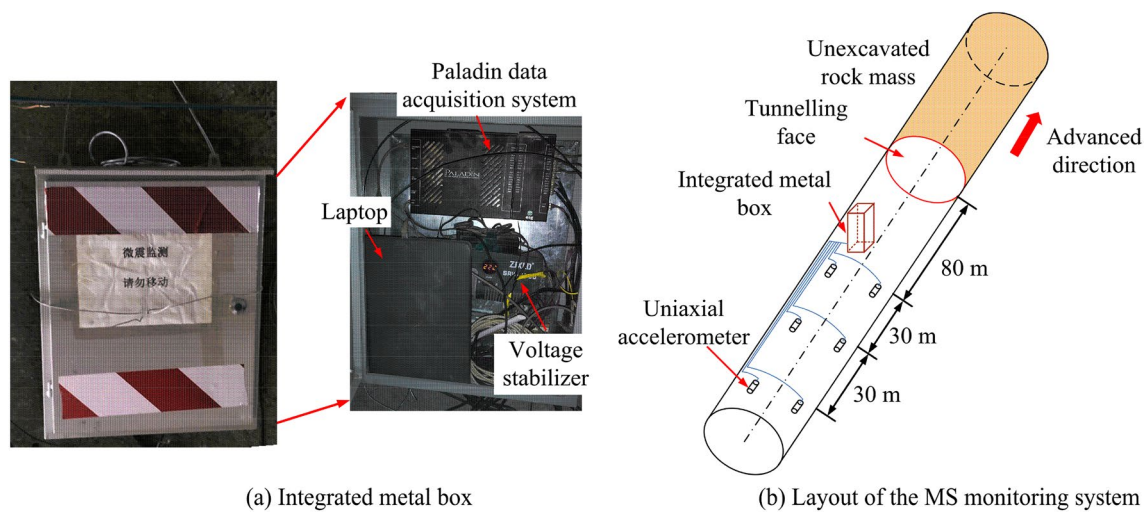


Fig. 5 Layout of MS monitoring system in the tunnel

### 2.3 Quantification of Source Parameters

The MS energy ( $E$ ) reflects the intensity of rock mass failure, which is calculated based on the recorded waveforms (Aki 1968; Boatwright and Fletcher 1984):

$$E = 4\pi\rho vR^2 \frac{J_c}{F_c^2} \tag{1}$$

where  $\rho$  is the rock density,  $v$  is the velocity of the body wave,  $R$  is the source radius,  $J_c$  is the energy flux (the integral of the particle motion velocity),  $F_c$  is the average radiation coefficients for the radiation type of the seismic waves. Moreover, some typical source parameters were adopted to evaluate stress level and seismic inelastic deformation of surrounding rocks. The apparent stress ( $\sigma_\alpha$ ) is defined as the average stress associated with seismic radiation resistance (Snoke et al. 1983):

$$\sigma_\alpha = \frac{\mu E}{M_0} \tag{2}$$

where  $\mu$ ,  $E$  and  $M_0$  respectively represent shear modulus, MS energy, and seismic moment. The volume of surrounding rocks with the source inelastic deformation is represented by apparent volume ( $V_\alpha$ ) (Mendecki 1993; Wyss and Brune 1968):

$$V_\alpha = \frac{M_0}{2\sigma_\alpha} = \frac{M_0^2}{2\mu E} \tag{3}$$

Moreover, local stress level of the failure sources is represented by energy index ( $EI$ ). It refers to the ratio of the measured radiated seismic energy to mean energy

radiated by events of the same seismic moment (Dai et al. 2016; Van Aswegen and Butler 1993):

$$EI = \frac{E}{\bar{E}(M_0)} \tag{4}$$

where  $\bar{E}(M_0)$  is the mean radiated energy. The  $\bar{E}(M_0)$  is calculated according to the relationship between  $\log E$  and  $\log M$ :

$$\log \bar{E}(M_0) = a \log M_0 + b \tag{5}$$

where  $a$  and  $b$ , fitting constant, can be obtained from the linear fitting of the MS energy and seismic moment. In seismology, the  $EI$  has a positive correlation with the apparent stress. Therefore, in following section, the MS energy, apparent volume, and energy index were used to investigate MS characteristics.

## 3 MS Event Characteristic

### 3.1 Temporal Distribution of MS Events

During the monitoring period from 13 May, 2022 to 5 July, 2022, a total of 1266 MS events were recorded. The count of MS events of per day has significant differences, e.g., 70 events and 1 event corresponding to 17 June and 28 June respectively (Fig. 6). In addition, there is no obvious correlation between the occurrence of rockburst and the count of MS event. Figure 7 shows the distribution of MS events occurring. The percentage of MS events occurring during the TBM tunneling is approximately 83.9 (Fig. 7a). For the other



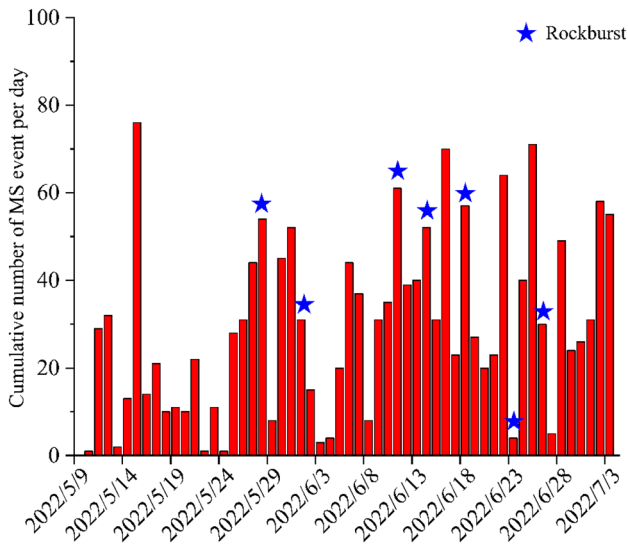


Fig. 6 Temporal evolution of MS events

MS events (16.1%), as the time from the last tunneling cycle increases, the count of MS events decreases. Analyzing the evolution characteristic of the MS events, it is found that the count of the MS event exponentially decreases as the time from the last tunneling cycle increases (Fig. 7b). The fitting coefficient is 0.89. Most of the MS events occur within 15 min after the tunneling cycle completed. This implies that within a short time after the excavation completed, the rock mass fracturing activity is still severe. If the MS event frequently occurs, especially for the intense rockburst segment, workers should not enter the operation area for construction work after one tunneling cycle completed until 15 min later.

### 3.2 Spatial Distribution of MS Events

On the top left corner and the lower right corner of the tunnel (i.e., from 9 o'clock to 12 o'clock, and from 3 o'clock to 5 o'clock (facing tunneling face)), small-scale structural planes

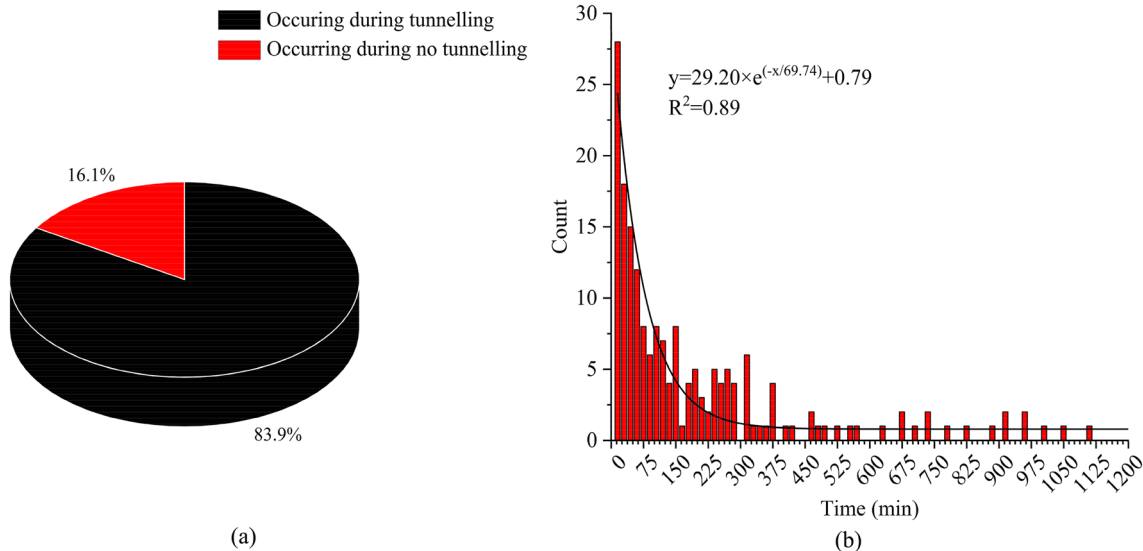
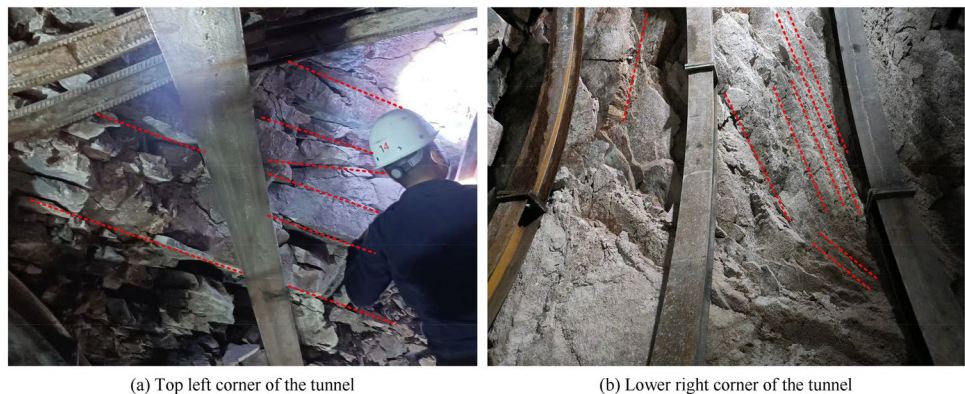


Fig. 7 Relationship between the MS event and TBM tunnelling: a proportional distribution; b distribution of the MS events occurring time to the last tunneling cycle (MS events occurring during no tunnelling)

Fig. 8 Surrounding rocks of the studied mileages



develop well (Fig. 8). The stress tends to concentrate near the zones of these small-scale structural planes under the action of excavation disturbance. Most of MS events are located in the top left corner and the lower right corner of the tunnel. Figure 9 shows the MS event distribution around the tunnel. If the location of MS event is in front of the tunneling face, the distance is a positive value. If the location is in behind of the tunneling face, the distance is a negative value. As the distance to the tunneling face increases, the number of MS event decreases, which mainly ranges from  $-15$  to  $15$  m (Fig. 9a). And these MS events present a normal distribution. The average value and the standard deviation respectively correspond to  $6.24$  m and  $9.03$  m, implying that more MS events occur in front of the tunneling face.

The distribution of the location of the MS events around the tunnel axis is shown in Fig. 9b. The tunnel axis corresponds to  $0$  m, and tunnel left and right correspond to the positive and negative values respectively. The ratio is the distance of MS event location to the tunnel axis to the tunnel diameter ( $6.53$  m). As the distance to the tunnel axis increases, the number of the MS event decreases, mainly distributing with approximate  $2.0$  times of the tunnel diameter. The MS events present a normal distribution, the average value and standard deviation respectively corresponding to  $0.96$  m and  $1.39$  m. The number of the MS event located in left side of the tunnel is larger than that in right side of the tunnel, which results from the structural planes more developed in the left side.

### 3.3 Energy Analysis

According to the field geological survey and MS energy, the level of MS events was divided into five levels,  $0-1$  kJ, slight level event,  $1-30$  kJ low level event,  $30-100$  kJ intermediate level event,  $100-800$  kJ high level event, and  $> 800$  kJ

extremely high level event. The number of event energy ranging from  $0$  to  $1$  kJ accounts for approximately  $34.8\%$  (Fig. 10a). That with  $30-100$  kJ accounts for the largest percentage, approximately  $47.8\%$ . As the energy ranging from  $100$  to  $800$  kJ, the percentage is the smallest, approximately  $5.6\%$ . Figure 10b shows the relationship between the cumulative MS event number per day and cumulative energy per day (taking logarithm). It is found that the cumulative event number has a linear correlation with the cumulative energy. While, the correlation is not obvious, fitting coefficient equal to  $0.29$ . It implies that the more active MS activity does not mean the occurrence of high-energy events. Therefore, it does not accurately predict a rockburst solely according to the event energy or event number per day.

Energy index and apparent volume have been widely used to predict rockbursts. The evolution characteristics of the energy index and apparent volume can reflect the stress state and deformation state of surrounding rock. The increase of the energy index indicates the increase of the stress level of surrounding rocks. The increase of the apparent volume means the deformation of surrounding rock of failure sources increases. When the energy index increases to a high level, the surrounding rock is close to failure. After that, the energy index begins to decrease, the apparent volume rapidly increases, and the surrounding rock appears a large deformation. Therefore, the rapid increase of the energy index accompanied by the increase of apparent volume can be used as one of the early warning indicators of large deformation of surrounding rock. In addition, if the MS activity is active, the MS energy should rapidly increase. In the present study, these three parameters are adopted to study rockburst development process. To calculate these parameters (the calculation method please refer to Sect. 2.3), the relationship between the  $\log M$  and  $\log E$  is primarily calculated, which is plotted in Fig. 11a. Then the cumulative energy

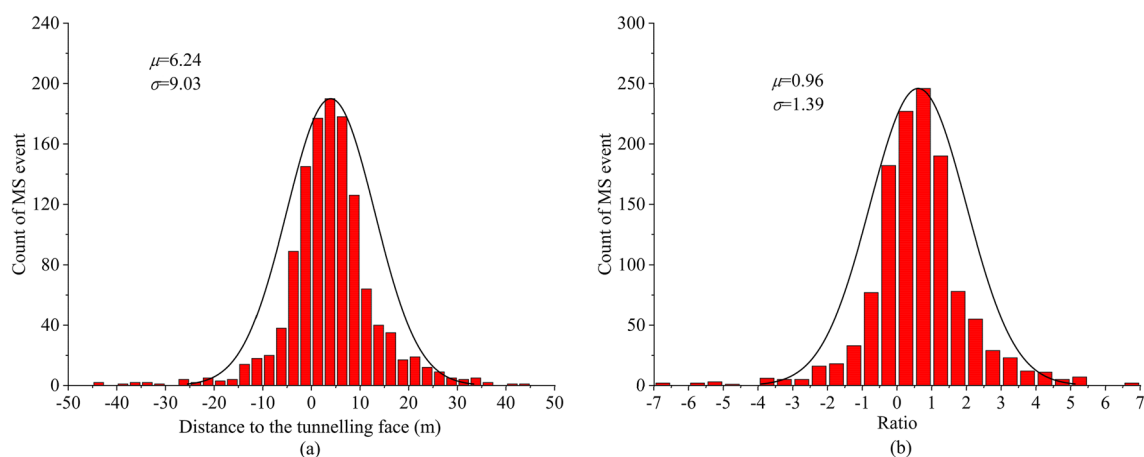


**Fig. 9** Location of MS events: **a** distance to the tunneling face; **b** ratio of the distance to the tunnel axis to the tunnel diameter (“ $\mu$ ” and “ $\sigma$ ” represent the average value and standard deviation, respectively.)

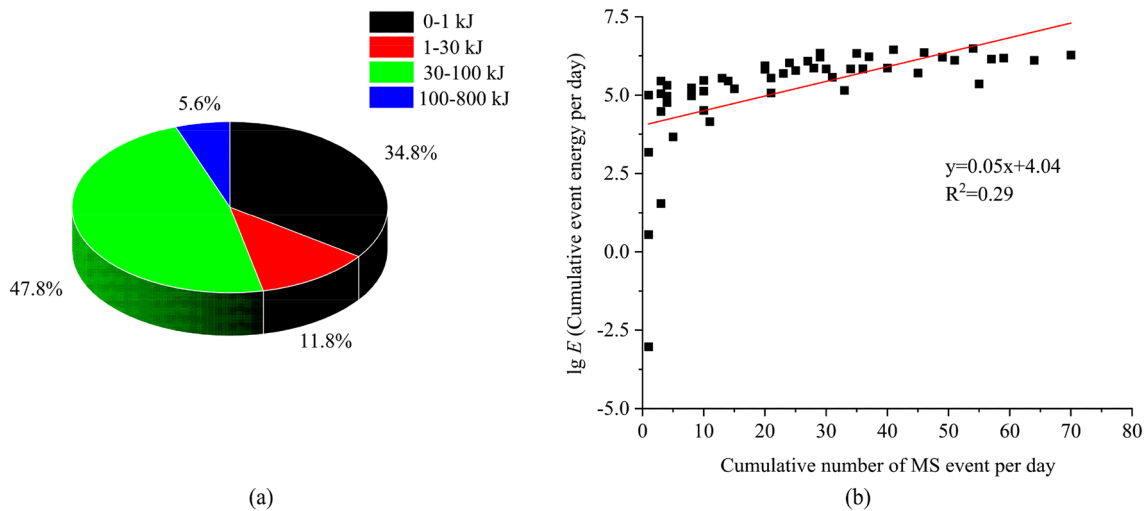


**Fig. 10** Energy of MS events: **a** percentage distribution of different energy levels; **b** relationship between the cumulative event number per day and cumulative energy per day

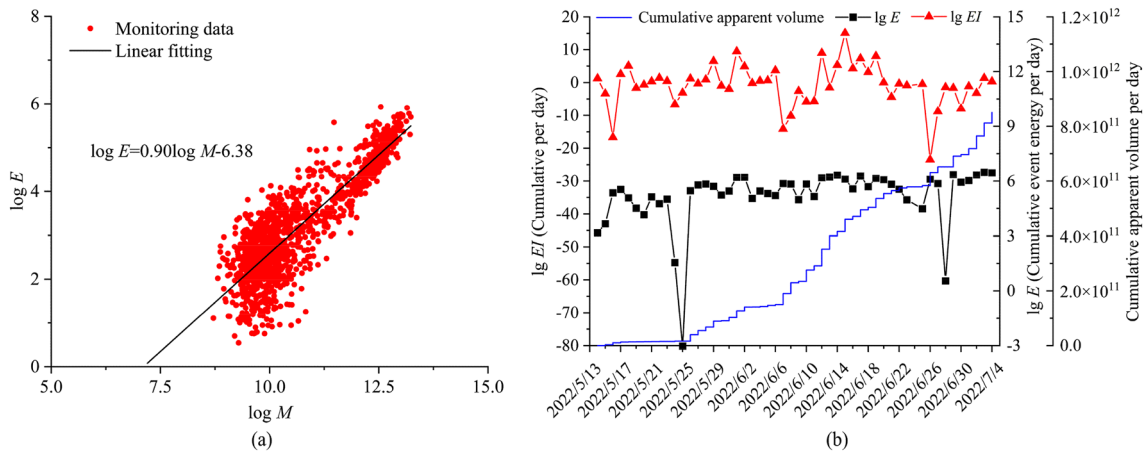


**Fig. 11** Energy parameters: **a** relationship between  $\log M$  and  $\log E$ ; **b** evolution process of the cumulative apparent volume, cumulative energy index per day ( $\lg EI$ ), and cumulative energy per day ( $\lg E$ )

index and energy per day, and the cumulative apparent volume are calculated. Figure 11b shows evolution process of the energy index, apparent volume, and energy versus date. From 13 to 26 May, the cumulative apparent volume increases slowly, implying the surrounding rock stable. From 26 May to 6 June, the cumulative apparent volume increases gradually, implying that the deformation of surrounding rocks gradually increases. These mileages correspond to the moderate rockburst segment. From 6 June to 5 July, the cumulative apparent volume rapidly increases, implying that surrounding rocks have large deformation. These mileages correspond to the intense rockburst segment. The cumulative apparent volume can well reflect the rockburst levels of different mileages. During the period of the rapid increase of cumulative apparent volume, the rapid decrease

of cumulative energy index occurs three times, corresponding to 7 June, 21 June, and 26 June, respectively. During these three days, the MS activity is active and some mild rockbursts occur. While no intense rockburst occurs. However, from 6 June to 5 July, several intense rockbursts occur (in Fig. 6). It implies that according to the cumulative energy index per day, these rockbursts cannot accurately predict. In addition, the cumulative energy per day is less sensitive to changes of the apparent volume.

In previous studies (Du et al. 2022; Ma et al. 2015; Yang et al. 2022; Yin et al. 2021), the cumulative energy index per day, cumulative energy per day, and cumulative apparent volume can well predict rockburst. While in the present study, these parameters cannot. It is because that in previous studies the rockburst was generally controlled by



a large-scale structural plane or several sets of structural planes. Before the rockburst occurs, MS events usually accumulate in an area over a period of time (one day or several days). Therefore, these cumulative parameters can well predict the rockburst. However, the small-scale structural planes in the present study develop well and there is no main-controlled structural plane. The occurrence of the rockburst is more sudden, and the accumulation trend within a day is not so obvious.

### 3.4 Rockburst Prediction

The energy index and the energy of each MS event are calculated and taken logarithm to predict rockbursts. According to the decrease of energy index and the increase of cumulative apparent volume, it cannot directly predict a rockburst (Fig. 11b). To directly predict the rockburst, a prediction index ( $k_{pi}$ ) is proposed based on the apparent volume and the energy index:

$$k_{pi} = \begin{cases} k_v \times k_{ei}, k_v > 0 \text{ and } k_{ei} < 0 \\ 0, \text{ others} \end{cases} \quad (6)$$

$$k_v = \frac{i + 1_{V_\alpha} - i_{V_\alpha}}{t_{i+1} - t_i} \quad (7)$$

$$k_{ei} = \frac{i + 1_{EI} - i_{EI}}{t_{i+1} - t_i}$$

where  $i_{V_\alpha}$  is the normalized apparent volume of the  $i$ th MS event,  $t_i$  is the time, and  $i_{EI}$  is the normalized energy index of the  $i$ th MS event. As the  $k_v$  is larger than 0 and the  $k_{ei}$  is less than 0, it means that the apparent volume and energy index begin to increase and decrease. Therefore, a high value (the absolute value) of the prediction index ( $k_{pi}$ ) means more likely occurrence of a rockburst. For other conditions (including  $k_v > 0$  and  $k_{ei} > 0$ ,  $k_v < 0$  and  $k_{ei} > 0$ , and  $k_v < 0$  and  $k_{ei} < 0$ ), a rockburst unlikely occurs and the prediction index ( $k_{pi}$ ) is set as 0. Moreover, if the energy index changes to the energy, the prediction index based on the energy is proposed:

$$k_e = \frac{i + 1_E - i_E}{t_{i+1} - t_i} \quad (8)$$

where  $i_E$  is the normalized energy of the  $i$ th MS event.

Figure 12 shows the evolution process of the energy of MS event, prediction index based on energy (Index-E) and energy index (Index-EI). The blue pentagram indicates occurring an intense rockburst. It is clear that most of the prediction index based on the event energy (marked by black triangle) is equal to 0. As the value of the Index-E is less than -10, an Index-E corresponds to a rockburst, which accurately corresponds to 4 rockbursts. During this period, seven

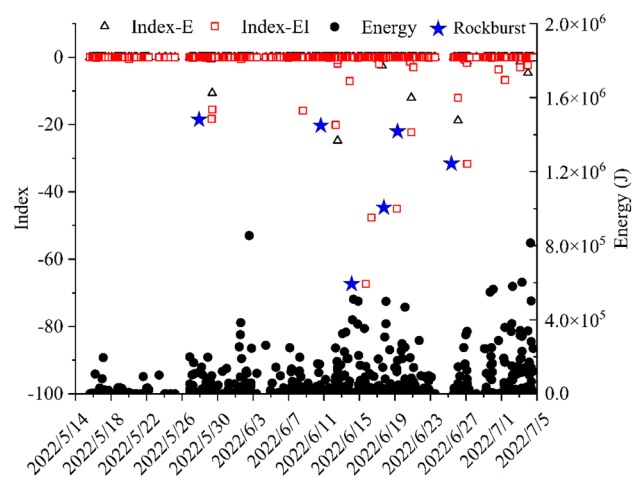


Fig. 12 Evolution process of MS event energy, prediction index based on energy (Index-E) and energy index (Index-EI)

intense rockbursts were recorded. The predication accurate rate is approximately 57.14%. For the predication index based on the energy index, as the value of the Index-E is less than -10, six rockbursts are accurately predicted. The predication rate is up to 85.71%. Therefore, the prediction index based on the energy index is recommended to using in this project to predict the intense rockburst.

Based on the ratio of S-wave to P-wave energy ( $E_s/E_p$ ), the failure mechanism of seismic sources can be distinguished (Xiao et al. 2016a):

$$\begin{cases} E_s/E_p < 10 & \text{Tensile failure} \\ 10 \leq E_s/E_p \leq 20 & \text{Mixed failure} \\ 20 < E_s/E_p & \text{Shear failure} \end{cases} \quad (9)$$

where  $E_s$  and  $E_p$  are the S-wave energy and P-wave energy respectively. The  $E_s/E_p$  value of these MS events is shown in Fig. 13. These MS events can be divided into three segments, i.e., mild rockburst segment, moderate rockburst segment, and intense segment. In the mild rockburst segment, most of the  $E_s/E_p$  ranges from 0 to 10. The percentage of the tensile failure, mixed failure and shear failure respectively corresponds to 96.8%, 2.4%, and 0.8% (Fig. 14). The tensile failure is predominated. The surrounding rocks are relatively stable, not slipping along the structural plane. For the moderate rockburst segment, the value of the ratio increases, and the percentage of the mixed failure and shear failure increases. The percentage of the tensile failure, mixed failure and shear failure respectively corresponds to 89.3%, 5.4%, and 5.3%. The surrounding rocks are unstable and at risk of failure. Some surrounding rocks may slip along the small-scale structural plane. Several moderate rockbursts occur in shear failure accompanied by some shear failure events. For the intense rockburst segment, although the tensile failure is

**Fig. 13** Distribution of the ratio of S-wave energy to P-wave energy ( $E_s/E_p$ )

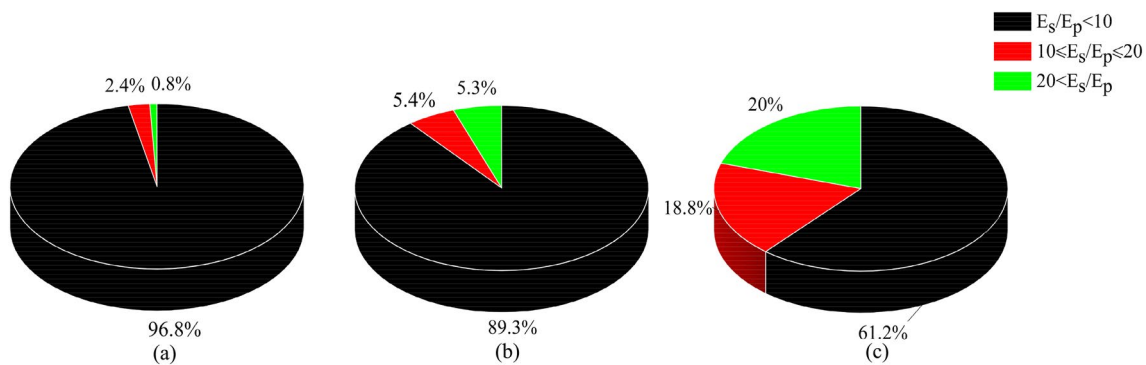
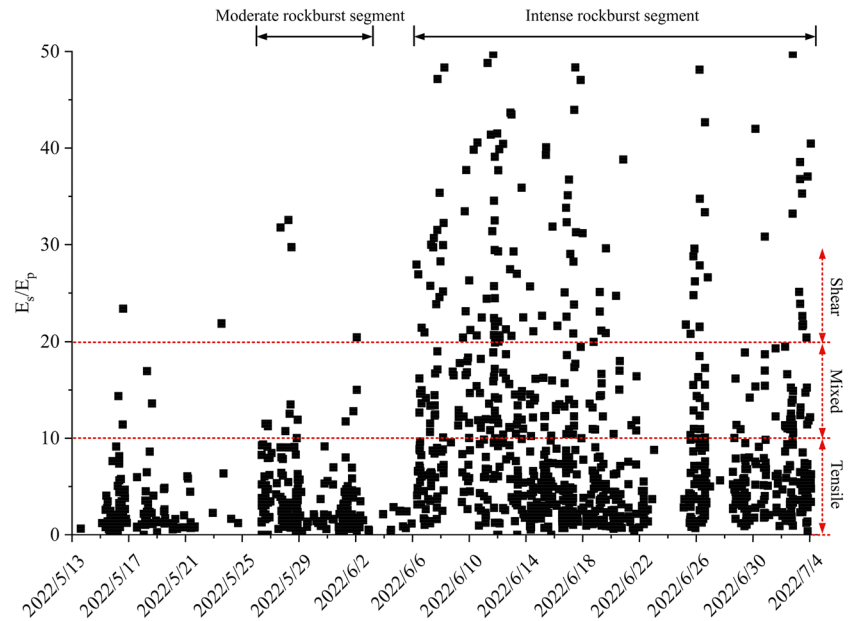


**Fig. 14** Percentage distribution of failure mechanism of MS events: **a** mild rockburst segment; **b** moderate rockburst segment; **c** intense rockburst segment

still predominated, the percentage of tensile failure sharply decreases and the percentage of mixed failure and shear failure rapidly increases. The percentage of tensile failure, mixed failure and shear failure respectively corresponds to 61.2%, 18.8%, and 20%. The surrounding rocks tends to unstable and slip along these small-scale structural planes. Some intense rockbursts occur in shear failure. From the above analysis, it is found that as the  $E_s/E_p$  value is less than 10, the surrounding rocks is relatively stable and few mild rockburst occur. As the  $E_s/E_p$  value rapidly increases, the surrounding rocks tends to unstable and some intense rockbursts occur. Therefore, the change in the  $E_s/E_p$  can be used as an indicator for warning the rockburst levels of different mileages.

## 4 Discussions

The tunneling parameters (e.g., penetration, cutterhead rotational speed, cutterhead thrust, and torque) can be directly read by TBM's driver. If the relationship between the tunneling parameters and intense rockburst is established, it can be better guidance for rockburst warning. Analyzing these tunneling parameters, i.e., penetration, cutterhead rotational speed, and torque, these do not have a significant change before an intense rockburst. While cutterhead thrust has an obvious change before an intense rockburst occurs. Figure 15 shows the evolution process of the thrust before four intense rockbursts. It is clear that before an intense rockburst occurs, the cutterhead thrust

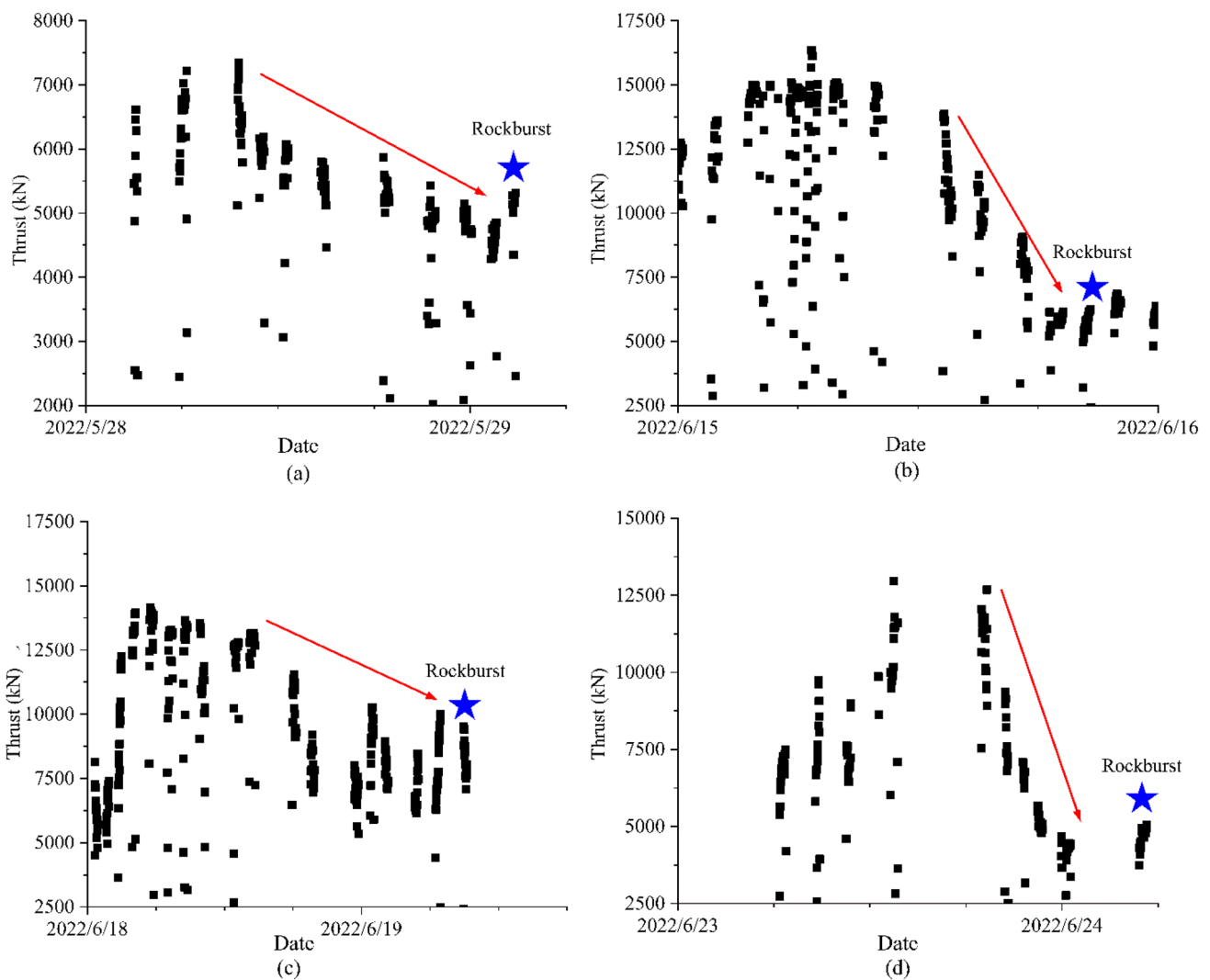


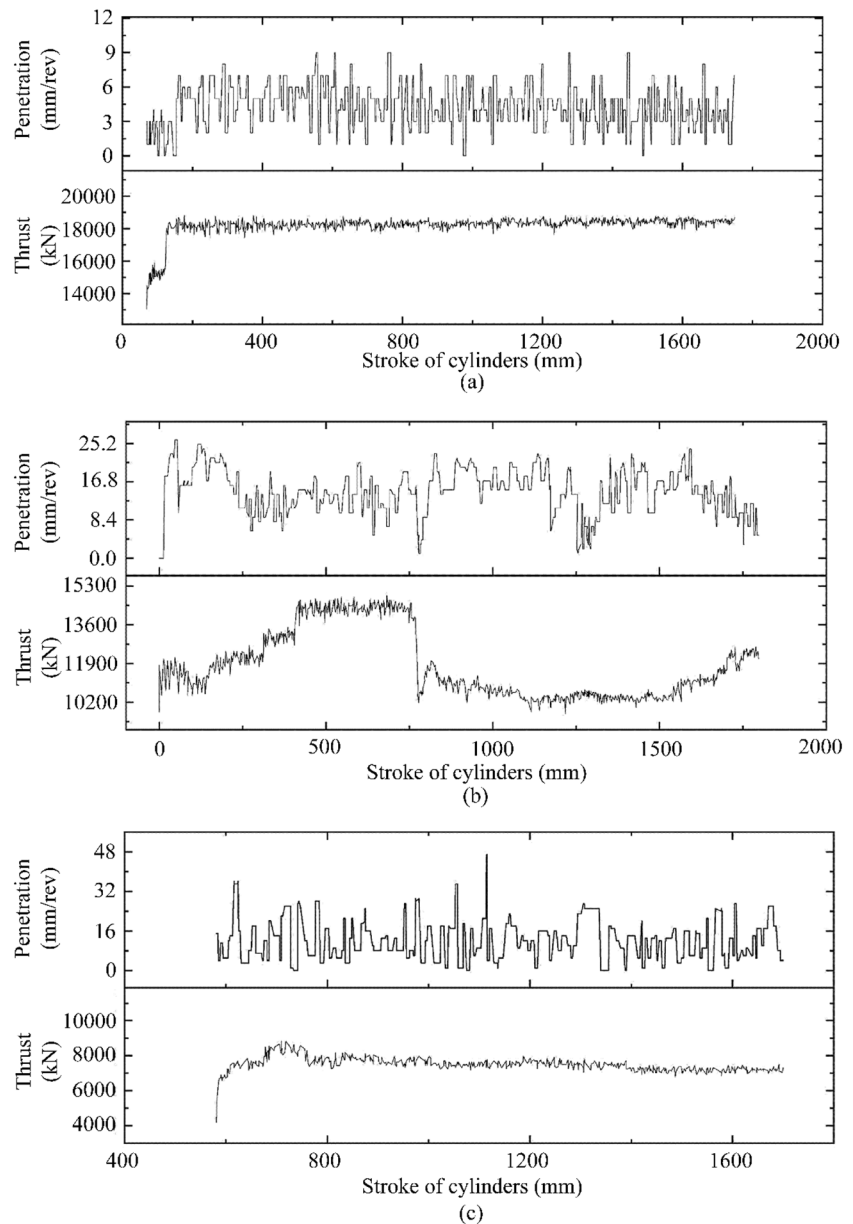
**Fig. 15** Evolution process of thrust before a rockburst: **a** 29 May rockburst; **b** 6 June rockburst; **c** 19 June rockburst; **d** 24 June rockburst

sharply decreases to approximately 5000 kN. Previous study (Lu et al. 2021) also observed this phenomenon. The states of stressed rock mass of tunneling face can be divided into 3 typical states, i.e., undamaged (meaning no brittle failure), slabbing/spalling, and rockburst (Fig. 16). For the undamaged tunneling face, the average penetration is small and stable (3–6 mm/rev), and the thrust ranges from 18,000 to 20,000 kN. For the slabbing in tunneling face, the average penetration and the thrust respectively have increase and decrease, corresponding to 13–14 mm/rev and 10,000–14000 kN. For the rockburst in tunneling face, the average penetration is approximately 13–14 mm/rev with the maximum 40 mm/rev, and the thrust decreases to 7000–8000 kN. It is because that a considerable number of rock fragments have been formed in the tunneling face, when a rockbursts occurs in the tunneling face. Due to the uneven tunneling face and large blocks, there

are some gaps between the cutterhead and the tunneling face, not closely contacted. The cutterhead thrust cannot be increased, regardless of the penetration or cutterhead rotational speed. Moreover, it is necessary to reduce the cutterhead thrust to ease the impact on the cutterhead and cutters and maintain the stability of tunneling face.

The changes of tunneling parameters could reflect the law of rockburst activity. Optimization of the tunneling parameters is an available operation for TBM to reduce rockburst hazards. In the present study, the relationship between rockburst and TBM excavation is qualitatively analyzed, in which a definite relationship has not been established. Future work is to collect more tunneling parameter data (including cutterhead penetration, thrust, torque, advance rate, and field penetration index) and rockburst cases. It should establish quantitative relationship between microseismicity and TBM

**Fig. 16** TBM tunneling parameters for different working conditions: **a** undamaged tunneling face; **b** slabbing/spalling in tunneling face; **c** rockburst in tunneling face. Modified from Lu et al. (2021)



excavation, which can provide guidance and reference for the early warning and treatment of rockbursts.

## 5 Conclusions

In the present study, a real-time MS monitoring system was established in a deep-buried tunnel to analyze MS event characteristic and evolution process of rockbursts. A prediction method was proposed to predict the rockburst. Conclusions can be drawn as follows:

1. The MS events mostly occur during the TBM tunneling, accounting for 83.9%. Other events occur during

the TBM shutting down period, which present an exponential decrease as the time increases and occur within 15 min after a tunneling cycle completed. The MS events mainly distribute within 15 m before and after the tunneling face, presenting a normal distribution based on the tunneling face. Moreover, the events mainly distribute within approximate 2.0 times of the tunnel diameter, presenting a normal distribution based on the central axis of the tunnel.

2. The cumulative energy parameter cannot accurately predict the rockburst, including the cumulative energy per day, cumulative energy index per day, with a forecast accuracy less than 60%. While the cumulative apparent volume can well classify the segment of rockburst level.



The prediction index based on the energy index per MS event and apparent volume per MS event can accurately predict the intense rockburst, with the forecast accuracy larger than 85%.

- The MS events of tensile failure are predominated, regardless of the mild rockburst segment, moderate rockburst segment, and intense rockburst segment. As the rockburst segment transits from mild to intense, the percentage of mixed failure and shear failure MS events sharp increases, especially shear failure events.

**Funding** The authors would like to thank the National Natural Science Foundation of China (Grant Nos. 52108382, 52378409, and 51978541), the Fundamental Research Funds for the Central Universities (Grant No. 2042022kf1054), and the State Key Laboratory of Geohazard Prevention and Geoenvironment Protection (Grant No. SKLGP2021K010) for funding provided to this work.

**Data Availability** The data that support the findings of this study are available on request from the corresponding author.

## Declarations

**Conflict of Interest** The authors declare that they have no conflict of interest.

## References

- Aki K (1968) Seismic displacements near a fault. *J Geophys Res* 73(16):5359–5376. <https://doi.org/10.1029/JB073i016p05359>
- Boatwright J, Fletcher JB (1984) The partition of radiated energy between *P* and *S* waves. *Bull Seismol Soc Am* 74(2):361–376. <https://doi.org/10.1785/BSSA0740020361>
- Cai M, Kaiser P, Martin C (2001) Quantification of rock mass damage in underground excavations from microseismic event monitoring. *Int J Rock Mech Min Sci* 38(8):1135–1145. [https://doi.org/10.1016/S1365-1609\(01\)00068-5](https://doi.org/10.1016/S1365-1609(01)00068-5)
- Chen G, Tang P, Huang RQ, Wang D (2020) Critical tension crack depth in rockslides that conform to the three-section mechanism. *Landslides* 18(1):79–88. <https://doi.org/10.1007/s10346-020-01471-x>
- Chen G, Li H, Wei T, Zhu J (2021) Searching for multistage sliding surfaces based on the discontinuous dynamic strength reduction method. *Eng Geol* 286(4):106086. <https://doi.org/10.1016/j.enggeo.2021.106086>
- Dai F, Li B, Xu N, Fan Y, Zhang C (2016) Deformation forecasting and stability analysis of large-scale underground powerhouse caverns from microseismic monitoring. *Int J Rock Mech Min Sci* 86:269–281. <https://doi.org/10.1016/j.ijrmmms.2016.05.001>
- Dai F, Li B, Xu N, Zhu Y (2017) Microseismic early warning of surrounding rock mass deformation in the underground powerhouse of the Houziyan hydropower station, China. *Tunnel Undergr Space Technol* 62:64–74. <https://doi.org/10.1016/j.tust.2016.11.009>
- Du C, Pan Y, Liu Q, Huang X, Yin X (2022) Rockburst inoculation process at different structural planes and microseismic warning technology: a case study. *Bull Eng Geol Environ* 81(12):1–18. <https://doi.org/10.1007/s10064-022-02980-w>
- Feng XT, Chen BR, Zhang CQ, Li SJ, Wu SY (2013) Mechanism, warning and dynamic control of rockburst development Process. Science Press, Beijing
- Feng GL, Feng XT, Chen BR, Xiao YX, Yu Y (2015) A microseismic method for dynamic warning of rockburst development processes in tunnels. *Rock Mech Rock Eng* 48(5):2061–2076. <https://doi.org/10.1007/s00603-014-0689-3>
- Feng GL, Feng XT, Xiao YX, Yao ZB, Hu L, Niu WJ, Li T (2019) Characteristic microseismicity during the development process of intermittent rockburst in a deep railway tunnel. *Int J Rock Mech Min Sci* 124:104135. <https://doi.org/10.1016/j.ijrmmms.2019.104135>
- Gibowicz S, Young R, Talebi S, Rawlence D (1991) Source parameters of seismic events at the underground research laboratory in Manitoba, Canada: scaling relations for events with moment magnitude smaller than -2. *Bull Seismol Soc Am* 81(4):1157–1182. <https://doi.org/10.1785/BSSA0810041157>
- Kaiser PK, McCreath D, Tannant D (1996) Canadian rockburst support handbook. Laurentian University, Geomechanics Research Centre, Sudbury
- Liu QS, Wu J, Zhang XP, Tang LX, Bi C, Li WW, Xu JL (2020) Microseismic monitoring to characterize structure-type rockbursts: a case study of a TBM-excavated tunnel. *Rock Mech Rock Eng* 53(7):2995–3013. <https://doi.org/10.1007/s00603-020-02111-5>
- Lu CP, Liu Y, Zhang N, Zhao TB, Wang HY (2018) In-situ and experimental investigations of rockburst precursor and prevention induced by fault slip. *Int J Rock Mech Min Sci* 108:86–95. <https://doi.org/10.1016/j.ijrmmms.2018.06.002>
- Lu J, Gong Q, Yin L, Zhou X (2021) Study on the tunneling response of TBM in stressed granite rock mass in Yinhan Water Conveyance tunnel. *Tunnel Undergr Space Technol* 118:1–12. <https://doi.org/10.1016/j.tust.2021.104197>
- Ma T, Tang C, Tang L, Zhang W, Wang L (2015) Rockburst characteristics and microseismic monitoring of deep-buried tunnels for Jinping II Hydropower Station. *Tunnel Undergr Space Technol* 49:345–368. <https://doi.org/10.1016/j.tust.2015.04.016>
- Małkowski P, Niedbalski Z (2020) A comprehensive geomechanical method for the assessment of rockburst hazards in underground mining. *Int J Min Sci Techno* 30(3):345–355. <https://doi.org/10.1016/j.ijmst.2020.04.009>
- Mendecki AJ (1993) Keynote address: real time quantitative seismology in mines. In: Proceedings of Third International Symposium on Rock-bursts and Seismicity in Mines 16–18 August 1993. Kingston, Ontario, Canada. pp 287–295
- Najm SJ, Daraei A (2023) Forecasting and controlling two main failure mechanisms in the Middle East's longest highway tunnel. *Eng Fail Anal* 146:107091. <https://doi.org/10.1016/j.engfailanal.2023.107091>
- Ortlepp W (2000) Study of rockburst source mechanism. Safety in mines research advisory committee. GAP 524:1–42
- Rehbock-Sander M, Jesel T (2018) Fault induced rock bursts and micro-tremors—experiences from the Gotthard base tunnel. *Tunnel Undergr Space Technol* 81:358–366. <https://doi.org/10.1016/j.tust.2018.07.003>
- Roy J, Eberhardt E, Bewick R, Campbell R (2023) Application of data analysis techniques to identify rockburst mechanisms, triggers, and contributing factors in cave mining. *Rock Mech Rock Eng*. <https://doi.org/10.1007/s00603-022-03206-x>
- Si Y, Liu J, Li F, Shi H, Yan G, Song J, Zhang C (2023) Experimental and theoretical investigation of roadway fracture induced by static-blast loading using acoustic emission. *Eng Fail Anal* 143:106909. <https://doi.org/10.1016/j.engfailanal.2022.106909>
- Snoke J, Linde A, Sacks I (1983) Apparent stress: an estimate of the stress drop. *Bull Seismol Soc Am* 73(2):339–348. <https://doi.org/10.1785/BSSA0730020339>

- Su G, Ren H, Jiang J, Hu X (2023) Experimental study on the characteristics of rockburst occurring at the working face during tunnel excavation. *Int J Rock Mech Min Sci* 164:105347. <https://doi.org/10.1016/j.ijrmms.2023.105347>
- Tang Z, Liu X, Xu Q, Li C, Qin P (2018) Stability evaluation of deep-buried TBM construction tunnel based on microseismic monitoring technology. *Tunnel Undergr Space Technol* 81:512–524. <https://doi.org/10.1016/j.tust.2018.08.028>
- The National Standards Compilation Group of People's Republic of China (2008) Code for engineering geological investigation of water resources and hydropower (GB50487-2008). China Planning Press, Beijing
- Van Aswegen G, Butler A (1993) Applications of quantitative seismology in South African gold mines. In: *Proc 3rd Int Symp on Rockbursts and Seismicity in Mines*, A.A. Balkema, Rotterdam, pp 261–266
- Wang Y, Ca T, Tang L, Zhang S, Li L, Li Y, Duan W (2021) Microseismicity characteristics before and after a rockburst and mechanisms of intermittent rockbursts in a water diversion tunnel. *Rock Mech Rock Eng* 55(1):341–361. <https://doi.org/10.1007/s00603-021-02666-x>
- Wyss M, Brune JN (1968) Seismic moment, stress, and source dimensions for earthquakes in the California-Nevada region. *J Geophys Res* 73(14):4681–4694. <https://doi.org/10.1029/JB073i014p04681>
- Xiao YX, Feng XT, Feng GL, Liu HJ, Jiang Q, Qiu SL (2016a) Mechanism of evolution of stress–structure controlled collapse of surrounding rock in caverns: a case study from the Baihetan hydropower station in China. *Tunnel Undergr Space Technol* 51:56–67. <https://doi.org/10.1016/j.tust.2015.10.020>
- Xiao YX, Feng XT, Li S, Feng G, Yu Y (2016b) Rock mass failure mechanisms during the evolution process of rockbursts in tunnels. *Int J Rock Mech Min Sci* 83:174–181. <https://doi.org/10.1016/j.ijrmms.2016.01.008>
- Xu N, Li T, Dai F, Zhang R, Tang C, Tang L (2016) Microseismic monitoring of strainburst activities in deep tunnels at the Jinping II hydropower station China. *Rock Mech Rock Eng* 49(3):981–1000. <https://doi.org/10.1007/s00603-015-0784-0>
- Xu J, Jiang J, Xu N, Liu Q, Gao Y (2017) A new energy index for evaluating the tendency of rockburst and its engineering application. *Eng Geol* 230:46–54. <https://doi.org/10.1016/j.enggeo.2017.09.015>
- Yang B, He M, Zhang Z, Zhu J, Chen Y (2022) A new criterion of strain rockburst in consideration of the plastic zone of tunnel surrounding rock. *Rock Mech Rock Eng* 55(3):1777–1789. <https://doi.org/10.1007/s00603-021-02725-3>
- Yao Z, Fang Y, Zhang R, Pu S, Zhao G, Yu T, Ma C (2023) The mechanism of stick–slip as a rockburst source in jointed rockmass: an experimental study. *Rock Mech Rock Eng*. <https://doi.org/10.1007/s00603-023-03220-7>
- Yin X, Liu Q, Pan Y, Huang X (2021) A novel tree-based algorithm for real-time prediction of rockburst risk using field microseismic monitoring. *Environ Earth Sci* 80(16):1–19. <https://doi.org/10.1007/s12665-021-09802-4>
- Zhou J, Li X, Mitri HS (2018) Evaluation method of rockburst: state-of-the-art literature review. *Tunnel Undergr Space Technol* 81:632–659. <https://doi.org/10.1016/j.tust.2018.08.029>
- Zhu H, Yan J, Liang W (2019) Challenges and development prospects of ultra-long and ultra-deep mountain tunnels. *Engineering* 5(3):384–392. <https://doi.org/10.1016/j.eng.2019.04.009>

**Publisher's Note** Springer Nature remains neutral with regard to jurisdictional claims in published maps and institutional affiliations.

Springer Nature or its licensor (e.g. a society or other partner) holds exclusive rights to this article under a publishing agreement with the author(s) or other rightsholder(s); author self-archiving of the accepted manuscript version of this article is solely governed by the terms of such publishing agreement and applicable law.